Sensitivity of the oceanic carbon reservoir to tropical surface wind stress variations

Author/Contributor:
Ridder, Nina; Meissner, Katrin; England, Matthew

Publication details:
Geophysical Research Letters
v. 40
Chapter No. 10
pp. 2218-2223
0094-8276 (ISSN)

Publication Date:
2013

Publisher DOI:
http://dx.doi.org/10.1002/grl.50498

Sensitivity of the oceanic carbon reservoir to tropical surface wind stress variations

N. N. Ridder,[1] K. J. Meissner,[1] and M. H. England[1]

Received 19 March 2013; revised 21 April 2013; accepted 22 April 2013; published 31 May 2013.

[1] The impact of variations of the Walker cell on the ocean carbon cycle is assessed using a coupled climate model. Idealized wind perturbations are investigated, with the trade winds increased/decreased by 10%, 20%, and 30%. A global-mean reduction in oceanic carbon storage is found for increased equatorial easterlies, while moderately decreased trade winds give increased uptake. There is a nonlinear response to weakened tropical winds due to Pacific Ocean biological pump changes; with reduced nutrient upwelling resulting in decreased biological activity and remineralization in the deep ocean. This partially offsets the increased carbon uptake due to weaker trade winds. The overall change in net carbon storage reaches –26.2 PgC (12 ppm) in the 30% increase case and 4.2 PgC (–2 ppm) in the 20% decrease cases. Regional dissolved inorganic carbon (DIC) changes reach –3.3 mmol m^{-3} (2.1 mmol m^{-3}) in the 10% decrease (increase) case. Gradually increasing wind perturbations give a similar pattern of DIC response to the full equilibrated solution. **Citation:** Ridder, N. N., K. J. Meissner, and M. H. England (2013), Sensitivity of the oceanic carbon reservoir to tropical surface wind stress variations, *Geophys. Res. Lett.*, *40*, 2218–2223, doi:10.1002/grl.50498.

1. Introduction

[2] The ocean is the major sink for anthropogenic carbon while also being the biggest carbon reservoir, holding approximately 93% of all exchangeable carbon in the Earth system [*Solomon et al.*, 2007]. The properties that govern the ocean's ability to take up carbon at the atmosphere-ocean interface comprise the following: (1) the partial pressure difference of CO_2 between atmosphere and ocean (ΔpCO_2), (2) the solubility of CO_2 in sea water, and (3) the gas transfer coefficient, or gas piston velocity. These parameters are influenced by various processes, the most important being (1) the surface wind stress that directly affects the gas transfer coefficient, (2) sea surface temperature (SST), which determines the solubility of carbon in sea water, (3) biogeochemical processes, for instance net primary productivity (NPP), that acts to remove carbon from the surface ocean and thus determine ΔpCO_2, and (4) ocean circulation processes, which can act to remove or add carbon-rich waters from/to the surface ocean. Subduction and deep convection, for instance, can remove carbon from the surface ocean and transport it into the deep ocean, thus facilitating further uptake of atmospheric carbon in today's climate. Upwelling of deep carbon-rich waters to the ocean surface in contrast can lead to CO_2 outgassing acting to counter the net oceanic uptake of anthropogenic CO_2. Furthermore, vertical transport within the ocean determines the nutrient supply to marine ecosystems, which plays an important role in the removal of carbon from the atmosphere and the surface ocean via the biological pump.

[3] All of the aforementioned processes are predicted to be modified in some way under the influence of global climate change (e.g., reviewed in *Houghton et al.* [2001]; *Solomon et al.* [2007]). The partial pressure difference for instance is changing due to anthropogenic emissions while the seawater solubility of CO_2 is being altered due to changes in SST, with solubility varying inversely with temperature [*Watson et al.*, 1995]. Ocean circulation and the gas transfer coefficient are also likely to change due to projected changes in the strength and position of wind fields in a warming climate and changes to surface buoyancy fields [e.g., *Russell et al.*, 2006; *Vecchi and Soden*, 2007; *Collins et al.*, 2010; *Tokinaga and Xie*, 2011; *Tokinaga et al.*, 2012]. The Walker circulation for instance has been estimated to have decreased over the past six decades under the observed global temperature increase as a result of a reduction in the mean sea level pressure gradient across the Pacific [*Collins et al.*, 2010; *Tokinaga et al.*, 2012]. Model studies predict this negative trend to persist into the future [*Vecchi and Soden*, 2007; *Collins et al.*, 2010]. They further predict a decrease in the equatorial trade winds and therefore zonal surface wind stress in warmer climates [e.g., *Vecchi and Soden*, 2007] by 0.003 N m^{-2} $°C^{-1}$ [*Collins et al.*, 2010]. This decrease in the easterly trade winds is not limited to the Pacific region [*Tokinaga and Xie*, 2011]; the equatorial easterlies in the Atlantic have also been estimated to have decreased over the past six decades and model studies predict a further weakening [*Vecchi and Soden*, 2007]. The reduction in surface wind stress is expected to lead to significant changes in SST, a weakening of ocean surface westward currents and equatorial upwelling, as well as a shoaling of the mean thermocline depth [e.g., *Philander*, 1981; *McPhaden*, 1993; *Clarke and Lebedev*, 1996; *Vecchi and Soden*, 2007]. It is therefore likely that such a modification of the trade winds will affect the ocean carbon cycle via ocean circulation changes, wind speed changes, SST changes and the resultant biogeochemical response.

[4] Paleoclimate records of Pacific Ocean SST suggest that such a change in zonal trade winds already occurred in the Pliocene (3.3–3.0 Ma) [*Haywood et al.*, 2005;

Additional supporting information may be found in the online version of this article.

[1]Australian Research Council Centre of Excellence for Climate System Science, University of New South Wales, Sydney, New South Wales, Australia.

Corresponding author: N. N. Ridder, Australian Research Council Centre of Excellence for Climate System Science, University of New South Wales, Level 4 Mathews Building, Sydney, NSW 2052, Australia. (n.ridder@unsw.edu.au)

0094-8276/13/10.1002/grl.50498

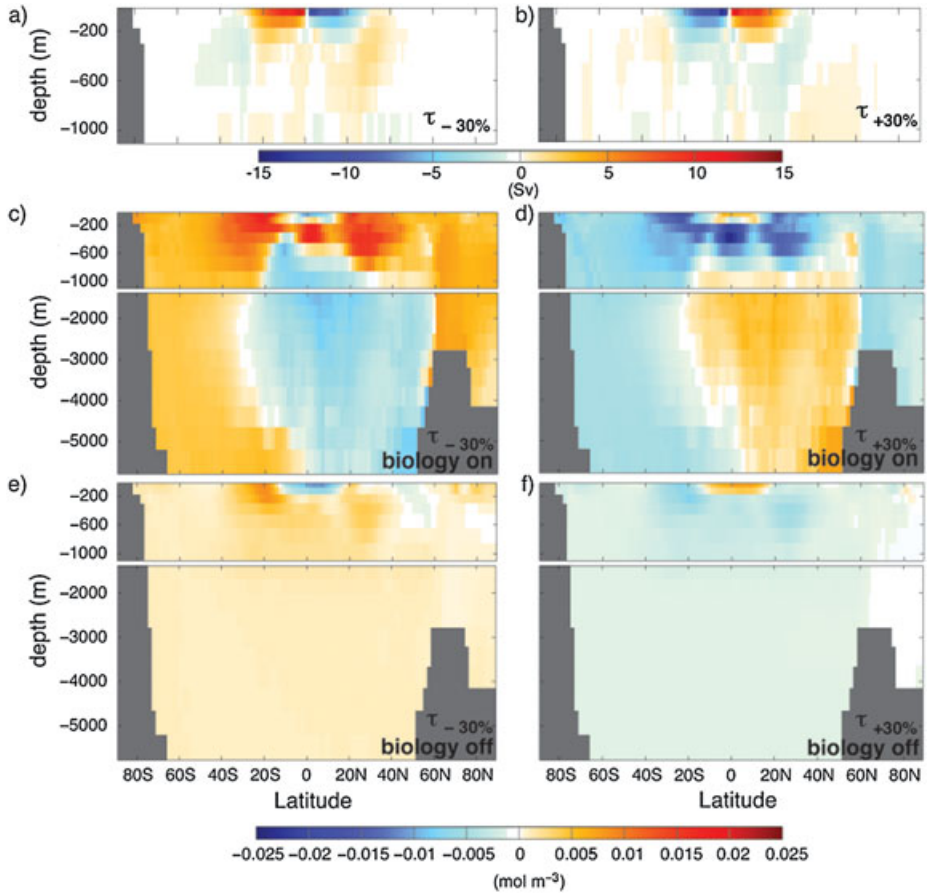

Figure 1. (a) Difference in annual mean MOC (Sv) in the upper 1000 m between $\tau_{-30\%}$ and CTRL; (c) annual mean zonal DIC changes (mol m^{-3}) between $\tau_{-30\%}$ and CTRL; (e) same as Figure 1c, but for experiments without marine biology; (b, d, f) same as in Figures 1a, 1c, and 1e, respectively, only for $\tau_{+30\%}$ minus CTRL.

Ravelo et al., 2006; *Shukla et al.*, 2009]. Analysis of paired $\delta^{18}O$ and magnesium-to-calcium ratio measurements from the tropical Pacific show that the east Pacific thermocline was deeper during the Pliocene and the east-to-west SST gradient across the Pacific was significantly weaker than during modern, non-ENSO conditions [*Wara et al.*, 2005]. It is now believed that the modern-day SST gradient in the equatorial Pacific developed during the cooling at the end of the Pliocene [e.g., *Ravelo et al.*, 2006]. The timing of the shoaling of the thermocline and the increase in the east-west temperature gradient during the mid-Pleistocene transition suggests that sustained long-term shifts in the tropics could play an important role in the evolution of the global climate on longer time scales [*Ravelo et al.*, 2006]. Even though it is commonly accepted that oceanic high latitude processes are the main drivers of major climate shifts through fluctuations in atmospheric CO_2 [e.g., *Sigman et al.*, 2010], these findings could hint to a more active role of the tropical Pacific in the control of the global climate state and atmospheric CO_2. With this and keeping in mind the integral role of the low-latitude Pacific Ocean in the atmosphere's heat balance [*Cane*, 1998], low-latitude processes have to be considered when investigating the drivers of global climate transitions.

[5] Given the possibility of past and future modifications of the Walker cell, we undertake here a sensitivity study to examine the response of the ocean carbon cycle to changes in the strength of the zonal equatorial surface wind stress by factors of ±10%, ±20%, and ±30% between 30°N and 30°S in the Pacific, the Atlantic, and the Indian Ocean. The focus here is on the long-term equilibrated carbon cycle response.

2. Model and Experimental Design

[6] The study employs the University of Victoria Earth System Climate Model (UVic ESCM, Version 2.9) [*Weaver et al.*, 2001]. The model consists of the ocean global circulation model (OGCM) MOM2.2, with a zonal resolution of 3.6° and a meridional resolution of 1.8° [*Pacanowski*, 1995]. Ocean circulation is forced by monthly mean reanalysis winds from the National Centers for Environmental Prediction (NCEP) [*Kalnay et al.*, 1996]. The OGCM is coupled to a two-dimensional energy-moisture balance model of the atmosphere, a thermodynamic/dynamic sea-ice model [*Semtner*, 1976; *Hibler*, 1979; *Hunke and Dukowicz*, 1997], a land surface scheme, a vegetation model (TRIFFID) [*Meissner et al.*, 2003], and a sediment model [*Archer*, 1996]. The UVic ESCM includes representations for both, biological [*Schmittner et al.*, 2008] and solubility cycling of carbon [*Ewen et al.*, 2004]. The UVic ESCM has been assessed against observational data and proven to be able to represent ocean properties, such as ocean circulation, temperature, and salinity as well as biological processes, reasonably well [e.g., *Meissner et al.*, 2003b; *Schmittner et al.*, 2008; *Meissner et al.*, 2012].

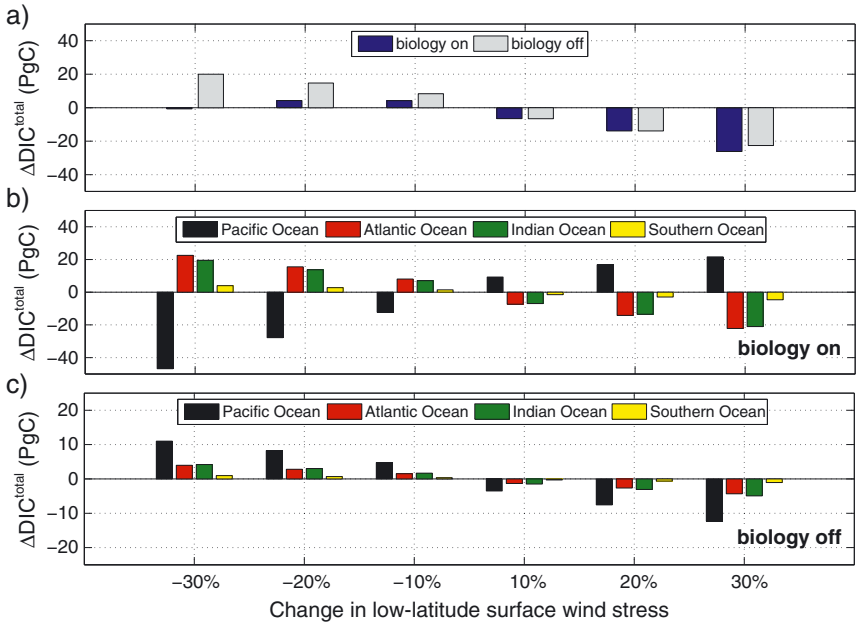

Figure 2. (a) Difference in annual mean global DIC (PgC) between the respective wind stress experiments and CTRL. Blue bars show changes in annual mean global total DIC using the full carbon cycle while grey bars represent annual mean changes for the respective experiment with marine biology model switched off. (b) Difference in annual mean total DIC content (PgC) in the different ocean basins between wind stress experiments and CTRL using the full carbon cycle; black (Pacific Ocean), red (Atlantic Ocean), green (Indian Ocean) and yellow (Southern Ocean); (c) same as Figure 2b with biology model switched off. Note that the range of the *y*-axis in Figure 2c is smaller compared to the range in Figures 2a and 2b to highlight changes; this is necessary due to the reduced carbon content in all experiments that exclude the biological carbon pump.

[7] For this study we integrate one control (CTRL) and six sensitivity simulations. CTRL is forced with NCEP reanalysis wind fields while the other scenarios are forced with either an increase (hereafter $\tau_{+10\%}$, $\tau_{+20\%}$ and $\tau_{+30\%}$) or a decrease (hereafter $\tau_{-10\%}$, $\tau_{-20\%}$ and $\tau_{-30\%}$) in the easterly component of the zonal surface wind stress (τ_x) by 10%, 20%, or 30% between 30°N and 30°S. The westerly wind component of the zonal surface wind stress field remains unchanged.

[8] All model scenarios are integrated with constant forcing until an equilibrium is reached. Atmospheric CO_2 concentrations are fixed to the year 2000 value of 369 ppm in all experiments. To investigate the changes in the oceanic carbon budget, oceanic carbon can be split into different components: saturation carbon (C^{sat}), disequilibrium carbon (ΔC), soft tissue (C^{soft}) and hard tissue carbon (C^{hard}) following a method summarized by *Williams and Follows* [2011]. Here we analyze changes in total dissolved inorganic carbon (DIC) as well as changes in C^{sat} and the circulation-driven component of ΔC only. This is achieved by switching the marine ecosystem model on or off for all simulations (including the control experiments). Via this method, we can isolate changes due to the solubility pump, affecting C^{sat} and the circulation-driven part of ΔC, from those due to the biological pump, affecting C^{soft} and C^{hard}. Note that the exclusion of marine biology leads to a reduced carbon content in the ocean throughout all experiments compared to the equivalent experiments including a biological model.

3. Vertical Distribution of DIC Changes

[9] The equatorial overturning cells show a clear weakening in response to the reduction in surface wind stress and a strengthening in the increased τ_x case; with changes varying between –13.6 Sv and 12.4 Sv (Figures 1a and 1b). The overturning in density coordinates shows equivalent results with maximum changes in the equatorial cells of –15.1 Sv and 13.5 Sv for experiments $\tau_{+30\%}$ and $\tau_{-30\%}$, respectively (not shown). The changes in the other major overturning cells, such as the North Atlantic Deep Water and Antarctic Bottom Water overturning cells, do not exceed 2 Sv (not shown). In the experiments with smaller wind perturbations, the overturning response exhibits similar patterns but with reduced magnitudes (not shown).

[10] The changes in zonal mean DIC at the surface and at depth at high latitudes are mostly of the same sign, except for over a region between the surface and ∼200 m depth at the Equator (Figures 1c and 1d). The main driver for this change is the solubility pump; in particular, changes in surface ocean temperatures, caused by a combination of decreased upwelling, reduced Ekman transport away from the equator and a reduction of the western boundary currents (compare Figures 1c and 1e). The resulting SST differences at high latitudes (cooling for decreased τ_x and vice versa for increased τ_x) alter the solubility of CO_2 in waters at regions of high ventilation depth (Figure S1, auxiliary material) and thereby affect the strength of the solubility pump as shown in Figures 1e and 1f. Note that the global oceanic carbon budget for CTRL without biology is much smaller than for the full model. Accordingly, changes are smaller in comparison to the full model too.

[11] The deep ocean between ∼20°S and ∼60°N and depths below ∼600 m in $\tau_{-30\%}$ (∼800 m in $\tau_{+30\%}$) exhibits changes of the opposite sign compared to the rest of the global ocean (Figures 1c and 1d) which are due to marine

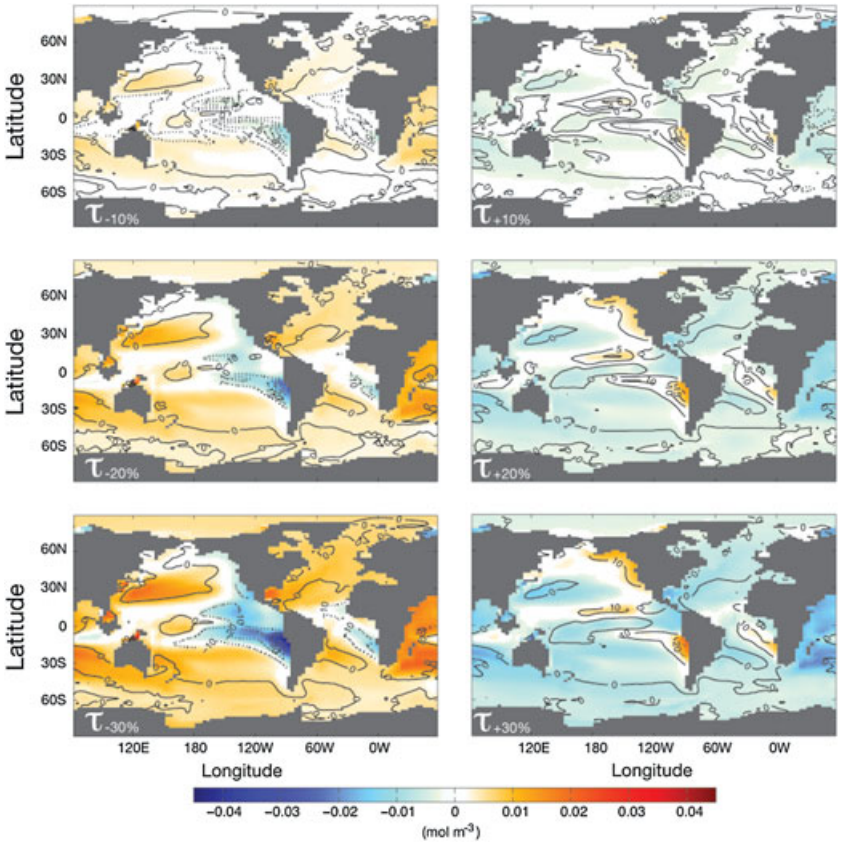

Figure 3. Changes in annual mean upper ocean (averaged between surface and 1000 m) DIC (color) and changes in annual mean upper ocean AOU (contours). (left column) Decreased surface wind stress experiments minus CTRL. (right column) Increased surface wind stress experiments minus CTRL. Contour intervals are 2 μM (top row), 5 μM (middle row) and 10 μM (bottom row), where 1 μM is 1 μmol l^{-1}.

biology. This can be seen by the lack of the DIC response differences in the deep ocean when the biological pump is suppressed compared to the experiments with biology (compare Figures 1c and 1d with Figures 1e and 1f). This is confirmed by an assessment of the nutrient to DIC upwelling ratio into the surface layer between 30°S and 30°N at the eastern boundary of each basin (Figure S2), which shows that the relative changes in nutrient upwelling exceed the relative changes DIC upwelling. Equivalent patterns of change, only less pronounced, can be found in the experiments with wind perturbations of ±10% and ±20% (not shown).

4. Global DIC Inventory Response

[12] In experiments with the biological pump switched off, the global carbon content scales with the changes in surface wind stress (grey bars in Figure 2a). This leads to an almost linear increase in net global DIC for decreased surface wind stress. A linear trend is also noted for the increased wind cases ($\tau_{+10\%}$, $\tau_{+20\%}$, and $\tau_{+30\%}$) in these pure solubility-pump experiments. Hence, overall, the net DIC in the solubility pump experiments varies inversely and linearly with tropical zonal wind stress strength. The model suggests maximum changes of up to 20 PgC ($\tau_{-30\%}$) and –24 PgC ($\tau_{+30\%}$), respectively. This response is in part due to changes in high-latitude SST, especially in regions of deep and intermediate water formation (Figure S1), resulting in variations in carbon solubility and thus the physical carbon pump.

[13] When biology is turned on, an increase in equatorial wind stress still leads to a reduction in global DIC in all experiments, which scales with the change in the wind stress and is slightly higher than the changes obtained when excluding biological impacts (compare blue to grey bars in Figure 2a). The response to a zonal wind stress decrease however is more complex and nonlinear. These changes indicate that the biological pump offsets the solubility pump under decreased τ_x conditions (Figure 2a).

[14] The nonlinear behavior described above derives exclusively from changes in the biological pump of the Pacific Ocean (black bars in Figures 2b and 2c), which exhibit total DIC changes of the opposite sign compared to all other ocean basins (Figure 2b). Furthermore, the total DIC change in the Pacific is twice as high for a decrease in τ_x compared to the equivalent increase in τ_x in the $\tau_{-30\%}$ and $\tau_{+30\%}$ experiments.

5. Response in the Biological Pump

[15] Overall, the changes in DIC averaged over the upper 1000 m correspond well to changes in apparent oxygen utilization (AOU; also averaged over the upper 1000 m; Figure 3). Focusing on the decreased surface wind stress experiments, the difference plots reveal an overall increase in the DIC concentration in all ocean basins. However, the

Pacific basin shows a clear decrease in the upper 1000 m at the eastern boundary of the basin. At the same time DIC increases at the western boundary of the North Pacific. This pattern is also seen at the depth of the 20° isotherm, which can be taken as a proxy for the depth of the pycnocline (Figure S3). A similar pattern evolves when the experiments are reconfigured to run as a transient perturbation, starting at zero and ramping up to maximum wind anomalies of ±10%, ±20%, ±30%, after 100 years (Figure S4). Similar patterns of change but of lower amplitude can be found in the Atlantic and the Indian Ocean, respectively. The experiments using an increased τ_x show the same pattern but with opposite sign (Figure 3, right column).

[16] The corresponding pattern of DIC and AOU changes gives a clear indication that the DIC changes are at least partly caused by changes in marine biological activity. As the DIC changes at the eastern boundary of each ocean basin are not present in the solubility pump experiments (Figure S5), solubility changes are not the cause of this feature of the DIC response to trade wind changes. In contrast, at the western boundary of the North Pacific and North Atlantic the solubility experiments do exhibit a similar increase in DIC, which suggests that the changes in these regions are caused by an interplay of both physical and biological processes.

[17] The changes in the eastern tropical ocean regions are caused by changes in upwelling of nutrients into the euphotic zone. Specifically, a decrease in τ_x leads to a decrease in upwelling, nutrient availability, NPP and remineralization (not shown) and therefore in DIC at depth, explaining the DIC changes seen in the intermediate and deep ocean at low latitudes (Figures 1c and 1d). This signal is consistent for all ocean basins and across all six wind perturbation experiments.

[18] The Humboldt Current Large Marine Ecosystem shows the response with highest magnitude, resulting in the higher sensitivity of Pacific Ocean carbon storage to changes in τ_x (Figure 2b). Overall, net upwelling across the 200 m interface in the equatorial Pacific Ocean varies between 34.6 Sv in $\tau_{+30\%}$ and 21.3 Sv in $\tau_{-30\%}$ compared to 27.6 Sv in CTRL. The Atlantic and Indian Oceans do include similar upwelling systems with net values at 200 m of 12.1 Sv and 13.7 Sv in CTRL, respectively. Here, however, the response of the total basin is dominated by the DIC changes outside of these upwelling regions due to the lower biological activity in these regions. This reverses the positive correlation between total DIC and τ_x seen in the Pacific into a negative correlation in the other ocean basins (Figure 2b). Net upwelling at 200 m in the Atlantic and the Indian ocean reaches maximum values of 10.4 Sv (14.4 Sv) in the Atlantic and 12.2 Sv (15.7 Sv) in the Indian Ocean in $\tau_{-30\%}$ ($\tau_{+30\%}$), respectively.

[19] The upwelling in the east Pacific is strongly influenced by the equatorial undercurrent (EUC) [*Rodgers et al.*, 2008]. Changes in the depth of isopycnal surfaces compared to the EUC can therefore alter the nutrient supply to this region. In a previous model study investigating the effect of changes in low latitude surface wind stress, *Rodgers et al.* [2008] described a decoupling between the pycnocline and the ferrocline in the equatorial Pacific. Here we find a similar decoupling. While the pycnocline in the equatorial Pacific changes in all sensitivity experiments (shoaling for increased and deepening for decreased wind stress conditions (Figures S6 and S7)), the mean depth of the nutricline remains almost unchanged (Figure S7). This alters the supply of nutrients to the east Pacific and contributes to the change in biological activity described above.

6. Summary and Conclusions

[20] This study assesses the impact of changes in tropical surface wind stress on the marine carbon cycle in a series of sensitivity experiments designed to assess the model response to idealized tropical wind perturbations. While an increase in low latitude surface wind stress leads to an almost linear decrease in total DIC, the changes induced by a decreased trade wind system show a nonlinear response. This should have implications for the future carbon cycle in response to ongoing warming and weakening of the Walker circulation [*Collins et al.*, 2010; *Tokinaga et al.*, 2012].

[21] Isolating the two carbon pumps reveals that the solubility pump forces each ocean basin in the same way and thereby leads to an approximate linear dependence of global DIC on equatorial zonal wind stress. The changes in the solubility pump are due to the changes in global ocean SST and circulation; in particular, a warming of high-latitude surface waters for strengthened τ_x conditions leading to decreased carbon solubility and vice versa for weaker equatorial trade winds.

[22] In the full carbon cycle experiments, the nonlinearity in the response to decreased τ_x conditions is caused by changes in Pacific Ocean productivity near the eastern boundaries. Weaker nutrient upwelling in $\tau_{-10\%}$, $\tau_{-20\%}$, and $\tau_{-30\%}$ leads to a decrease in NPP, which causes a decrease in the export of organic material to the deep ocean, resulting in decreased DIC formation through remineralization at depths at low- and mid-latitudes that offsets the solubility driven increases in carbon. The same interplay of the two competing pumps determines the total DIC change in the increased τ_x experiments. However, the changes in ocean productivity in the increased τ_x experiments are less pronounced and are unable to offset the linear changes driven by the alteration of carbon solubility.

[23] Overall, the processes determining the response of ocean carbon to changes in low latitude winds can be summarized as follows: The main driver behind all changes in both carbon pumps are modifications in ocean circulation, most importantly (a) the poleward transport of surface waters and (b) equatorial upwelling. Modifications in the poleward transport affect mid- and high-latitude SST, which respond with the same sign as the perturbation (i.e., increased winds, increased mid- to high-latitude SST). This cooling (warming) for decreased (increased) equatorial winds leads to changes in carbon solubility in seawater. This affects the solubility pump directly and is of the same sign in all ocean basins. On the other hand, modifications in equatorial upwelling lead to changes in the nutrient availability, and with this, net primary productivity, export production, and remineralization, i.e., the biological carbon pump. This results in changes in DIC at depths. This mechanism dominates the response of the Pacific Ocean in the reduced wind experiments. In all other ocean basins and under increased tropical wind conditions, the effect of this mechanism is small compared to changes in carbon solubility due to SST changes.

[24] In respect to past climate regimes, this study provides an estimate of the potential impact of low-latitude

wind changes on the global carbon cycle. In this study the focus was on the equilibrium response of the coupled climate system; a closer investigation of possible impacts due to potential changes in the Redfield ratio and atmospheric CO_2 feedbacks is left for future studies.

[25] In conclusion, this study sheds light on the carbon cycle response to altered tropical trade winds, showing that oceanic carbon uptake behaves in two competing ways to determine the net DIC response. This leads to an almost linearly decreasing total carbon content for increasing τ_x conditions, but a nonlinear response for equivalent wind stress reductions (Figure 2). With progressing climate change and if ongoing trends in the tropical trade wind strength continue, this has implications for the uptake, storage, and distribution of DIC in the respective ocean basins. However, the sign of the response, namely increased ocean carbon storage for decreased winds, implies a negative or self-limiting feedback. This suggests that the global atmospheric CO_2 response to tropical wind changes will be small, despite significant regional implications.

[26] **Acknowledgments.** This study was funded by the Australian Research Council (FL100100214 and FT10010043) and supported by an award under the Merit Allocation Scheme on the NCI National Facility at the Australian National University. N. Ridder was funded under the IPRS scheme of the Australian Government Department of Industry, Innovation, Science, Research and Tertiary Education. The authors thank Michael Eby for his engagement during the review progress, Rüdiger Gerdes for his helpful comments during final stages of this manuscript, and Willem Sijp for assistance in configuring the model experiments used in this study. The authors also thank two anonymous reviewers for their helpful comments.

[27] The Editor thanks two anonymous reviewers for their assistance in evaluating this paper.

References

Archer, D. (1996), A data-driven model of the global calcite lysocline, *Global Biogeochem. Cy.*, *10*(3), 511–526.

Cane, M. A. (1998), A role for the tropical Pacific, *Science*, *282*(5386), 59–61.

Clarke, A. J., and A. Lebedev (1996), Long-term changes in the equatorial Pacific trade winds., *J. Climate*, *9*, 1020–1029.

Collins, M., S. An, W. Cai, A. Ganachaud, E. Guilyardi, F. Jin, M. Jochum, M. Lengaigne, S. Power, A. Timmermann, G. Vecchi, and A. Wittenberg (2010), The impact of global warming on the tropical Pacific Ocean and El Niño, *Nat. Geosci.*, *3*, 391–397.

Ewen, T. L., A. J. Weaver, and M. Eby (2004), Sensitivity of the inorganic ocean carbon cycle to future climate warming in the UVic coupled model, *Atmos. Ocean*, *42*, 23– 42.

Haywood, A. M., P. Dekens, A. C. Ravelo, and M. Williams (2005), Warmer tropics during the mid-Pliocene? Evidence from alkenone paleothermometry and a fully coupled ocean-atmosphere GCM, *Geochem. Geophy. Geosy.*, *6*, Q03010, doi:10.1029/2004GC000799.

Hibler, W. D., III (1979), A dynamic thermodynamic sea ice model, *J. Phys. Oceanogr.*, *9*, 815–846.

Houghton, J. T., Y. Ding, D. J. Griggs, M. Noguer, P. J. van der Linden, X. Dai, K. Maskell, and C. A. Johnson (eds.) (2001), *Climate Change 2001: The Scientific Basis. Contribution of Working Group I to the Third Assessment Report of the Intergovernmental Panel on Climate Change*, 881 pp, Cambridge University Press , Cambridge, United Kingdom and New York, NY, USA.

Hunke, E. C., and J. K. Dukowicz (1997), An elastic viscous plastic model for sea ice dynamics, *J. Phys. Oceanogr.*, *27*, 1849.

Kalnay, E., et al. (1996), The NCEP/NCAR 40-year reanalysis project, *B. Am. Meteorol. Soc.*, *77*, 437–472.

McPhaden, M. J. (1993), TOGA-TAO and the 1991–93 El Niño-southern oscillation event, *Oceanography*, *6*(2), 36–44.

Meissner, K. J., A. J. Weaver, H. D. Matthews, and P. M. Cox (2003), The role of land surface dynamics in glacial inception: A study with the UVic Earth System Model, *Clim. Dynam.*, *21*, 515–537.

Meissner, K. J., A. Schmittner, A. J. Weaver, and J. F. Adkins (2003b), The ventilation of the North Atlantic Ocean during the Last Glacial Maximum—A comparison between simulated and observed radiocarbon age, *Paleoceanography*, *18*(2), 1023, doi:10.1029/2002PA000762.

Meissner, K. J., B. I. McNeil, M. Eby, and E. C. Wiebe (2012), The importance of the terrestrial weathering feedback for multimillennial coral reef habitat recovery, *Global Biogeochem. Cy.*, *26*, GB3017, doi:10.1029/2011GB004098.

Pacanowski, R. C. (1995), MOM 2 documentation: User's guide and reference manual, version 1.0, *GFDL Ocean Group Tech. Rep.*, *3*.

Philander, S. G. H. (1981), The response of equatorial oceans to a relaxation of the trade winds, *J. Phys. Oceanogr.*, *11*, 176–189.

Ravelo, A., P. Dekens, and M. McCarthy (2006), Evidence for El Niño-like conditions during the Pliocene, *GSA TODAY*, *16*(3), 4.

Rodgers, K. B., O. Aumont, C. Menkes, and T. Gorgues (2008), Decadal variations in equatorial Pacific ecosystems and ferrocline/pycnocline decoupling, *Global Biogeochem. Cy.*, *22*, GB2019, doi:10.1029/2006GB002919.

Russell, J. L., K. W. Dixon, A. Gnanadesikan, R. J. Stouffer, and J. R. Toggweiler (2006), The Southern Hemisphere westerlies in a warming world: Propping open the door to the deep ocean, *J. Climate*, *19*, 6382–3690.

Schmittner, A., A. Oschlies, H. D. Matthews, and E. D. Galbraith (2008), Future changes in climate, ocean circulation, ecosystems, and biogeochemical cycling simulated for a business-as-usual CO_2 emission scenario until year 4000 AD, *Global Biogeochem. Cy.*, *22*, GB1013, doi:10.1029/2007GB002953.

Semtner, A. J. J. (1976), A model for the thermodynamic growth of sea ice in numerical investigations of climate, *J. Phys. Oceanogr.*, *6*, 379–389.

Shukla, S. P., M. A. Chandler, J. Jonas, L. E. Sohl, K. Mankoff, and H. Dowsett (2009), Impact of a permanent El Niño (El Padre) and Indian Ocean Dipole in warm Pliocene climates, *Paleoceanography*, *24*, PA2221, doi:10.1029/2008PA001682.

Sigman, D. M., M. P. Hain, and G. H. Haug (2010), The polar ocean and glacial cycles in atmospheric CO_2 concentration, *Nature*, *466*(7302), 47–55.

Solomon, S., D. Qin, M. Manning, Z. Chen, M. Marquis, K. B. Averyt, M. Tignor, and H. L. Miller (eds.) (2007), *Contribution of Working Group I to the Fourth Assessment Report of the Intergovernmental Panel on Climate Change*, 996 pp., Cambridge University Press, Cambridge, United Kingdom and New York, NY, USA.

Tokinaga, H., and S.-P. Xie (2011), Weakening of the equatorial Atlantic cold tongue over the past six decades, *Nat. Geosci.*, *4*(4), 222–226.

Tokinaga, H., S.-P. Xie, A. Timmermann, S. McGregor, T. Ogata, H. Kubota, and Y. M. Okumura (2012), Regional patterns of tropical Indo-Pacific climate change: Evidence of the Walker circulation weakening, *J. Climate*, *25*, 1689–1710.

Vecchi, G. A., and B. J. Soden (2007), Global warming and the weakening of the tropical circulation, *J. Climate*, *20*, 4316.

Wara, M. W., A. C. Ravelo, and M. L. Delaney (2005), Permanent El Niño-like conditions during the Pliocene warm period, *Science*, *309*(5735), 758–761.

Watson, A., P. Nightingale, D. Cooper, H. Leach, M. Follows, A. Watson, P. Nightingale, D. Cooper, H. Leach, and M. Follows (1995), Modelling atmosphere-ocean CO_2 transfer [and discussion], *Philos. T. Roy. Soc. B*, *348*(1324), 125–132.

Weaver, A., et al. (2001), The UVic Earth System Climate Model: Model description, climatology and application to past, present and future climates, *Atmo Ocean*, *39*, 361– 428.

Williams, R., and M. Follows (2011), *Ocean Dynamics and the Carbon Cycle: Principles and mechanisms*, 404 pp., Cambridge University Press, Cambridge, United Kingdom and New York, NY, USA.